RSC Advances

ROYAL SOCIETY OF CHEMISTRY

www.rsc.org/advances

Adsorption studies of methyl orange on Mn-nanoparticle decorated organo-functionalized SiO_2-Al_2O_3 mixed-oxides: Kinetic, equilibrium and thermodynamic

M. Arshadi*, F. SalimiVahid[b], J.W.L. Salvacion[b], M. Soleymanzadeh[b]

[a]Department of Science, Fasa Branch, Islamic Azad University, PO Box 364, Fasa 7461713591, Fars, Iran

[b]Mapúa Institute of Technology, Muralla St. Intramuros, Manila 1002 Philippines

Abstract

In this paper a novel nano adsorbent containing Mn–nanoparticles decorated organo-functionalized SiO_2–Al_2O_3 mixed-oxides was introduced as a new scavenger of dyes such as methyl orange. SiO_2–Al_2O_3 mixed–oxides was functionalized with Schiff base ligand and thereatfer, in the next step, Mn–nanoparticle was prepared over the organo–functionalized SiO_2–Al_2O_3 mixed–oxides. The synthesized materials were characterized by several methods such as FT–IR spectroscopy, UV–vis, CHN elemental analysis, SEM, TEM, ICP–OES, EPR and XPS. The contact time to obtain equilibrium for maximum adsorption was 15 min. EPR and XPS of Mn ions evidenced that most of the covalently bond active sites of the nano-adsorbent are in the form of Mn(III) ions. The heterogeneous Mn(III) ions were found to be effective adsorbent for

* To whom correspondence should be addressed. Tel.: +989361528179.
E-mail Address: m-arshadi@ch.iut.ac.ir, mohammadarshadi@yahoo.com (M. Arshadi)

the removal of methyl orange ions from solution. The adsorption process was spontaneous and endothermic in nature and followed pseudo-second-order kinetic model.

Keywords: Nano-sized SiO_2-Al_2O_3, Mn nanoparticle, methyl orange, dye adsorption.

Introduction

Dyes pollution of wastewater is an environmental problem urgently needing to be solved. The sources of aquatic dyes pollution are broad; including numerous industries like the plastics, paper, textile and also cosmetics utilize dyes to color their goods and 15% of dyes are lost during the dyeing process. Dyes usually have a synthetic origin and complex chemical structure that make them persistence to light, oxidation and biodegrade process.[1] Indeed, numerous dyes were developed for their chemical invariability and do not suffer from biochemical degradation easily. Nowadays, more than one hundred thousand kinds of commercial dyes are utilized with a production of over nine million tons annually.[1,2] Therefore, improving a sustainable method for the removal of synthetic dyes has long been a challenge for scientists. In particular, many efforts have been made to develop several kinds of materials to remove dyes from drinking water.

The following conventional methods used in dyes removal from wastewater: coagulation and flocculation, oxidation or ozonation, membrane

separation, and adsorption.[2] Adsorption processes have been reported to be the low-cost promising alternatives for the treatment of dyes present in wastewater. The use of activated carbons, modified clays, polymeric resins, waste materials, and zeolites as adsorbents have also been described.[1,2] For most of natural adsorbents such as clays, zeolites, agricultural waste, and chitosan their particles show negatively charged surfaces and consequently, excellent adsorption properties for cationic organic compounds can be obtained. However, these systems generally have some disadvantages to dye removal, such as the difficulty in separating those powdery natural adsorbent, except high speed centrifugation, from treated effluent, nonresistance against acid solution, their poor mechanical strengths and less adaptable to a wide range of dye wastewaters limits their practical applications. However, most of these adsorbents either do not have considerable adsorption capacities or need relatively long adsorption contact times, e.g., from several hours to a couple of days (Table 1). It is, therefore, desired to develop effective adsorbents with short contact times for the removal of dye ions from aqueous solutions. Activated carbon is the most prevailing adsorbent for this process because of its high surface area, high adsorption capacity, and high degree of surface reactivity; however, it is expensive and must be regenerated on a regular basis. Inorganic supports present several advantages with respect to activated carbon, including stability, high surface area, possible reuse, relative rapidity in reaching equilibrium, better high mechanical resistance, easy modifications and

a higher concentration of chelating groups on the surface, and they are often much cheaper than their organic counterparts. For comparative purposes, the adsorption capacities of several adsorbents for methyl orange are summarized in Table 1.

In this paper, the application of a stable covalently immobilized Mn nanoparticles (manganese is one of the most versatile metals playing a central catalytic role in environment) on the surface of SiO_2–Al_2O_3 mixed–oxides host by a linker approach have been studied as a novel nano-adsorbent for the capturing methyl orange from aqueous solution. Methyl orange (M.O.) with IUPAC name of Sodium 4-[(4-dimethylamino) phenyl diazenyl] benzene sulfonate is a typical water-soluble anionic dye and has harmful effects on living organisms in a short period of exposure.

2. Experimental

2.1. Materials

All chemicals were purchased from Merck and Aldrich and used without further purification, except for solvents, which were treated according to standard methods. Doubly distilled water was used throughout.

Table 1. Adsorption Capacities of MO on Various Adsorbents.

Adsorbents	Q_{max} (mg g^{-1})	Reference
Ferrocene-Si/Al	381	3
λ-Fe2O3/MWCNTs/chitosan	60.5–66.1	4
Hypercrosslinked chloromethylated PS adsorbent functionalized with formaldehyde carbonyl groups (HJ-1)	70.9–76.9	5
Mesoporous magnetic Co-NPs/carbon nanocomposites	380	6
Acid modified carbon coated monolith	132.7	7
Calcined layered double hydroxides	200	8
Alkali-activated multiwalled carbon nanotubes	149	9
Pinecone derived activated carbon	404.4	10
carbon nanotubes	35.4–64.7	11
Chitin/alginate magnetic nano-gel beads (MCAs)	107.5	12
Porous spongy CSGO monolith	567.07	13
chitosan/MgO composite	60	14
Cu@Cu2O	344.8	15
ultrafine coal powder	5.24	16
modified ultrafine coal powder	5.56	16
Chitosan	34.83	17
Calcined Lapindo volcanic mud	333.3	18
Mesoporous Y-Fe2O3/SiO2 nanocomposites calcined	476	19
Y-Fe2O3/SiO2/chitosan composite	34.29	20
MgNiAl layered double hydroxides	375	21
Protonated cross-linked chitosan	89.30	22
mesoporous carbon CMK-3	294.1	23
De-Oiled Soya	16.66	24
Bottom Ash	3.61	24
metal-organic framework (MOF)	194	25
Ni-containing ordered mesoporous carbons	107.1	26
hypercrosslinked polymer	72.9	27
Banana peel	21	28
ammonium-functionalized silica nanoparticle	105.4	29
Palygorskite Clays	39	30
700 ^{o}C Treated Palygorskite Clays	98	30
Mn@Si/Al	571	This work

2.2. Preparation of the organometallic functionalized SiO_2–Al_2O_3 mixed-oxide

SiO_2–Al_2O_3 (1/1) was used as the support. This support was prepared by sol–gel method as follow; Aluminum tri–sec–butylate (97%) and tetraethyl orthosilicate (98%) were used as the precursors, and 2,4–pentandione (H–acac)

as the complexing agent. Appropriate amounts of aluminum tri–*sec*–butylate and tetraethyl orthosilicate were dissolved in *n*–butanol and the solution was heated to 60 °C. The components were thoroughly mixed, then it was cooled down to room temperature, and then H–acac was added. The produced clear solution was hydrolyzed with deionized water (11.0 mol H_2O/ mol alkoxide). The solution was left overnight to hydrolyze the alkoxides, yielding transparent gel. The transparent gel was dried at 110 °C to remove water and any solvent, and then it was calcined at 500 °C for 5 h to remove the organic materials. The support is referred as SiO_2–Al_2O_3 (1:1). The SiO_2–Al_2O_3 (1:1)-supported 2-aminoethyl-3-aminopropyl-trimethoxysilane (2–AE–3–APTMS) (Scheme 1) was prepared by refluxing 5.2 g SiO_2–Al_2O_3 (1:1) that was activated at 550 °C for 6 h under air with 3.5 mL (0.0195 mol) of 2–AE–3–APTMS in dry dichloromethane (100 mL) for 24 h. The solid was filtered and washed off with methanol, dichloromethane and dried at 100 °C under vacuum for 6 h. The functionalized SiO_2–Al_2O_3 (1:1) mixed-oxides that was prepared with the linker, is identified hereafter by Si/Al-*pr*-NH-*et*-NH_2. Then, methyl-2-pyridylketone was added to a suspended solution of Si/Al-*pr*-NH-*et*-NH_2 in dry methanol. The mixture was refluxed for 24 h to prepare a Schiff base (*vide* Scheme 1) on the surface of the mixed-oxides (a bi-dentate ligand).

The adsorbent containing Mn nanoparticles was obtained by stirring 0.5 g of the hybrid material, Si/Al mixed-oxides-Schiff base ligand, with Mn $(OCOCH_3)_2$ $4H_2O$ (5.4 mmol), and LiCl (8.5 mmol) in 30 mL of ethanol at

reflux for 24 h. Then, the resulting material (brown powder) was filtered off, washed with copious of ethanol and methanol and dried under vacuum at 60 °C.

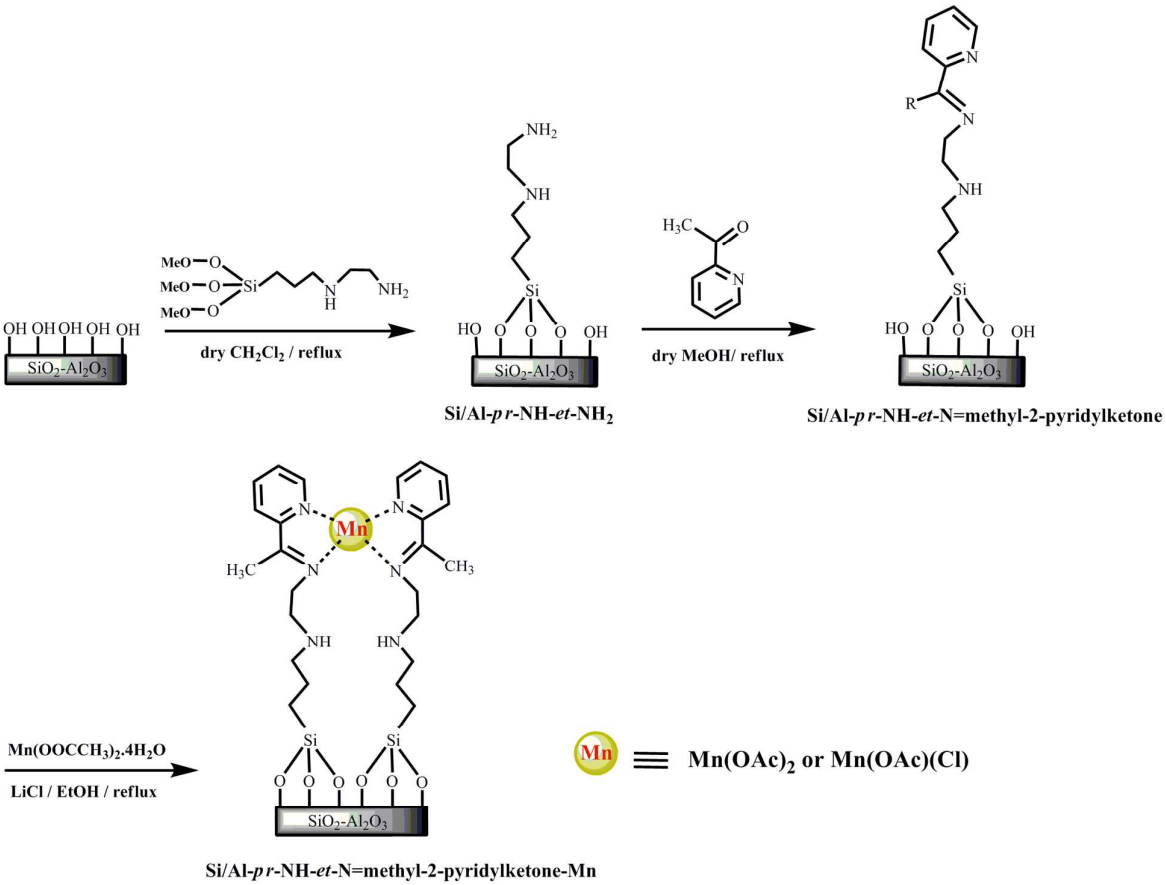

Scheme 1. Immobilization procedure of the organometallic functionalized SiO_2-Al_2O_3 mixed-oxides.

2.3. Characterization

Diffuse reflectance spectra were recorded on a JASCOV-550 UV–Vis spectrophotometer. Fourier transform IR spectra were measured using a JASCO FT/IR (680 plus) spectrometer. The spectra of solids were obtained using KBr pellets. The vibrational transition frequencies are reported in wave numbers

(cm^{-1}). Approximately 40-50 mg of material, which had been previously calcined in air at 298 K for 4 h, with 10-15 times KBr was pressed (for 3 min at 15 metric tons/cm^2 pressure under approximately 10-2 Torr vacuum) into a self-supporting wafer of 0.9 mm diameter. The FTIR spectra of synthesized materials were recorded at 4 cm^{-1} resolution and scan number of 16. Elemental analysis was performed by a CHNO-Rapid Heraeus elemental analyzer (Wellesley MA). Chemical analyses are carried out by inductively coupled plasma optical emission spectroscopy (ICP-OES) using a Shimadzu ARL 34000 instrument (spectroflamed; typically, 30 mg sample was dissolved in 500 µl 40% HF solution, 4 mL 1:4 HCl:H_2SO_4 solution and 45 mL H_2O). Nitrogen (99.999 %) adsorption experiments have been performed at -196 °C using a volumetric apparatus (Quanta chrome NOVA automated gas sorption analyzer). Before the adsorption experiments, the sample was out gassed at 120 °C for 16 h. The specific surface areas are calculated from the BET method. Transmission electron microscopy (TEM) was carried out on the powder samples with a Tecnai F30TEM operating at an accelerating voltage of 300 kV. In addition, energy dispersive X-ray analysis was conducted on each sample. XPS (small area X-ray photoelectron spectroscopy) data were recorded with the PHI-5702 Multi-Technique System. Electron paramagnetic resonance (EPR) spectra were recorded with a Bruker EMX spectrometer operating at X-band (m = 9.42 GHz) frequency and a 100 kHz field-modulation. The spectra were recorded at 80 K using a Bruker BVTB 3500 variable temperature controller. The magnetic field

was calibrated with a Bruker ER 035 M NMR gaussmeter and the microwave-frequency was calibrated with a frequency counter fitted in a Bruker ER 041 XG-D microwave bridge unit.

2.4. Adsorption measurements

Different MO ion concentrations were freshly prepared in a solution of deionized water. Sorption experiments were carried out in batch conditions: 0.07 g of Mn nano-adsorbent was shaken up with a 20 mL of the organic pollutant , at a concentration of between 0.75 and 1000 mg L^{-1}, at a controlled temperature box of 25 ºC (each reaction was repeated three times, and displayed a relative standard deviation lower than 1.64%). The time required to work in equilibrium condition was determined by preliminary kinetic measurements. The kinetic tests of MO showed no significant variation in sorption after 24 h. After centrifugation at 3000 rpm for 5 min the liquid phase was separated and the solute concentration was determined at λ_{max} = 464.0 nm using a JASCOV–550 instrument.

The amount adsorbed was calculated as:

$$q_e = V . (C_o - C_e) / m \quad (1)$$

where C_o and C_e are the initial and equilibrium liquid-phase concentrations ($mg \cdot L^{-1}$) of adsorbate; V is the volume of the solution (L); and m is the amount of adsorbent (g). Equation 1 assumes that the change in volume of the bulk liquid phase is negligible as the solute concentration is small and the volume occupied by the adsorbent is also small. The amount of the dye adsorbed on the sample was calculated based on a previously determined calibration curve.

3. Results and discussion

3.1. Characterization of Mn@Si/Al

The structures of the obtained organometallic–modified Si–Al mixed oxides was confirmed by elemental analysis, BET (N_2 adsorption–desorption technique), FT–IR spectroscopy, UV–Vis, SEM, TEM, ICP–MS, EPR and XPS. Nitrogen sorption measurement of the modified Si/Al mixed oxides confirms the presence of the Mn–complex attached to the modified Si/Al mixed oxides (Table 2). The considerable decrease of the specific surface area (S_{BET}) after functionalization is due to the presence of organometallic groups, which block the access of nitrogen molecules into the structure of the SiO_2–Al_2O_3 mixed oxides. The nitrogen and Mn contents of the organometallic–modified Si/Al mixed oxides (Mn@Si/Al) were determined by elemental analysis and ICP,

respectively. Consequently, the content of the immobilized Mn@Si/Al was computed. The results are listed in Table 2. From these data could calculate that the aluminosilicate support bearing 4.1 mmol g^{-1} of Schiff base and 3.0 mmol g^{-1} of Mn ions. In fact, during the condensation and immobilization, the dosage of methyl-2-pyridylketone was excessive to minimize the amount of the untreated residual linker on the support. A change in the color of the resulted powder can also be visualized during the reactions (scheme 1).

Table 2. Chemical composition and physicochemical properties of the organometallic functionalized SiO_2/Al_2O_3 mixed oxides.

Catalyst	Elemental analyses (wt%)[b]		Organic functional group (mmol/g mixed oxide)[c]	Immobilized Mn-Schiff base-complex (mmol/g mixed oxide)[d]	Structural parameters[e]		
	N	Mn			Surface area (m^2/g)	Pore volume (cm^3/g)	Pore diameter (A^o)
SiO_2/Al_2O_3 mixed oxide[a]	-	-	-	-	243	0.028	20
Si/Al-*pr*-NH-*et*-N=methyl-2-pyridylketone	6.2	-	4.4	-	131	0.014	16
Si/Al-*pr*-NH-*et*-N=methyl-2-pyridylketone-Mn	5.7	3.0	4.1	0.56	114	0.014	16

[a] Molar ratio of Si/Al was 60:40, determined from EDX analysis.
[b] Nitrogen was estimated from the elemental analyses. Mn content determined from ICP analysis.
[c] Determined from the N-contents.
[d] Determined from the Mn-content.
[e] The pore size calculated using the BJH method.

3.1.1. IR Spectroscopy

Infrared wave numbers (cm^{-1}) of significant valence vibrations, which are collected in Figure 1, are helpful for identification of the immobilized ligand and the complex. SiO_2–Al_2O_3 mixed oxide showed characteristic FT-IR peaks at 2900–3800, 1260–1060 and 600-900 cm^{-1} due to O–H of the $(Si/Al)O_4$ units, adsorbed water molecules and M–O–M stretching vibrations [31], respectively,

and also the bands at 2851–2921cm^{-1} are assigned to the stretching mode of the remained –CH_2 groups. 2–AE–3–APTMS-SiO_2–Al_2O_3 showed bands at 2851–2921cm^{-1} which strongly suggests that the SiO_2–Al_2O_3 mixed oxide has successfully been modified by amine spacer groups. Likewise, the N–H deformation peaks at 1540–1560 cm^{-1} confirm the successful functionalization of the Si/Al mixed oxides with 2–AE–3–APTMS. In accordance with previously reported data,[32] the C=N (Schiff base) absorption was assigned at the 1635 cm^{-1}, the vibration of C=N of pyridine group appeared in the region 1571–1569 cm^{-1} (Fig. 1) ,[33] and the peak at 1436 cm^{-1} can be assigned to C=C stretching vibration of pyridine group. The FT–IR spectrum of Schiff base clearly shows the C–H vibrations of Py groups at 3070–3060 cm^{-1}, which further confirming the presence of pyridine groups on the Si/Al mixed oxides after immobilization of the ligand.

In the infrared spectrum of the pristine SiO_2/Al_2O_3, the structural bands at 780 cm^{-1} were responsible for the stretching vibrations modes of M-O, M-O-M, and O-M-O bonds, where M means metal atoms, and O means oxygen atoms. Furthermore, it was seen that there were complex bands in the 780 cm^{-1} region, attributed to ring vibrational modes. It was interesting to note that the bands related to the M-O lattice vibrations are changed in their intensities around 780 cm^{-1}, where it was further indicated that organo functional group was successfully immobilized on SiO_2/Al_2O_3. However, for the spectra of Mn@Si/Al, it was easily seen that the bands were similar to those of SiO_2/Al_2O_3

in the range from 900 to 600 cm^{-1}, indicating that M-O lattice vibrations showed a small change. Further evidence for this coordination mode was provided by the ν(Mn–N) band at ca. 412 cm^{-1}.[34] The FT–IR results demonstrate the formation of the Mn–complex, immobilized on the Si/Al mixed oxides through 2–AE–3–APTMS linker (Fig. 1).

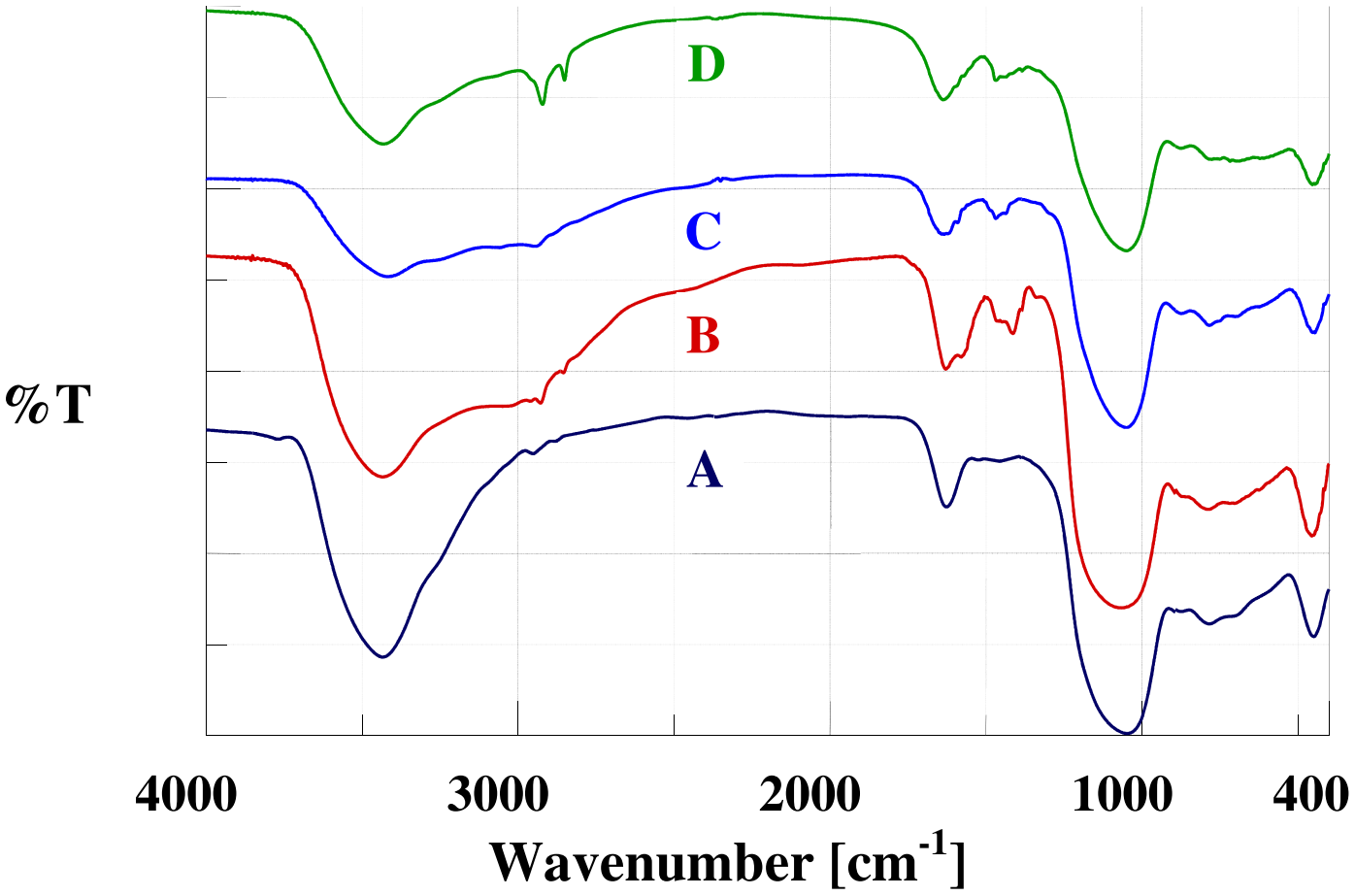

Figure 1. FT-IR spectra the organometallic functionalized SiO_2/Al_2O_3 mixed oxides in the region 4000-400 cm^{-1}. Legends: SiO_2/Al_2O_3 mixed oxides (A), Si/Al-*pr*-NH-*et*-NH_2 (B), Si/Al-*pr*-NH-*et*-N=methyl-2-pyridylketone (C), Si/Al-*pr*-NH-*et*-N=methyl-2-pyridylketone-Mn (D).

3.1.2. Dynamic Reflectance UV–Vis spectroscopy

Anchoring of the synthesized materials on the solid surface was also followed by DR UV–Vis spectroscopy of the resulting adsorbent. Thus, the UV–Vis spectrum of Si/Al mixed oxides only had a side-band adsorption near 244 nm, while the spectrum of the Si/Al–*pr*–NH–*et*–N=methyl–2–pyridylketone–Mn (Mn@Si/Al) was dominated by strong absorptions in the 250- 305 nm region due to the $\pi \rightarrow \pi^*$ and $n \rightarrow \pi^*$ transitions of the ligand (Fig. 2). Furthermore, the Mn@Si/Al exhibited the broad and weak bands around 391 nm, probably attributable to the ligand-to-metal charge transfer transitions, similar to the metallosalen compounds.[35] Several low intensity asymmetric broad band appeared over 500 nm in the visible region at λ = 530–680 nm are attributed to the d→d transitions; expected for the manganese complexes with a square pyramidal geometry, ($d_{xz} \rightarrow d_{x^2-y^2}$), ($d_{yz}$, $d_{xy} \rightarrow d_{x^2-y^2}$) and ($d_{z^2} \rightarrow d_{x^2-y^2}$) which were similar to the related metal (salen) compounds described in the literatures.[36] DR–UV–Vis and FT–IR spectra reveal that the Mn@Si/Al nano-adsorbent is synthesized upon coordination of Mn ions to the organo-functional groups. The charge transfer bands, the stretching frequency at 1635 cm^{-1} (Fig. 1) and elemental analyses (Table 1) clearly confirm that the Schiff base ligands and C=N groups are not affected or destroyed through the immobilization on the functionalized Si/Al mixed oxides.

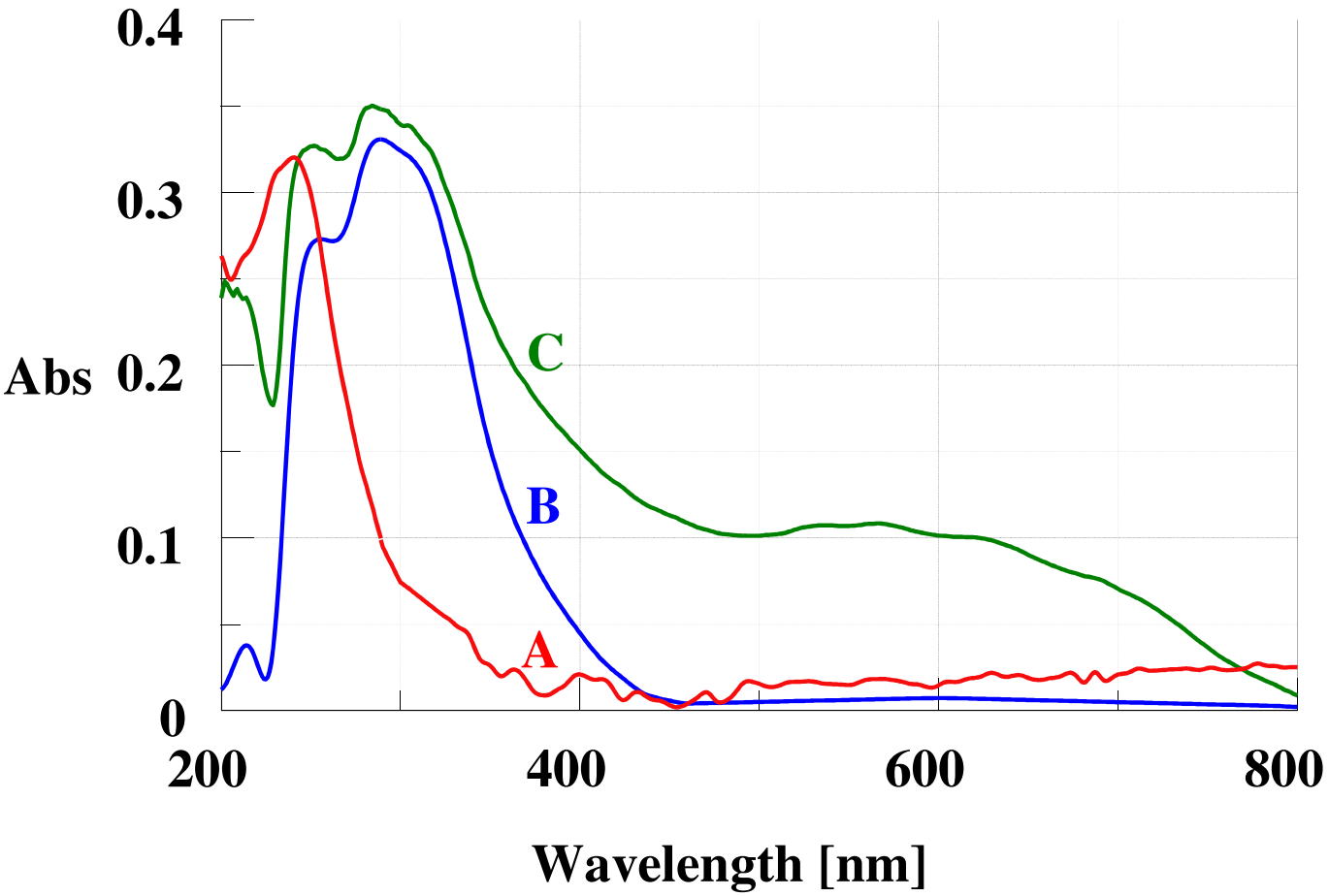

Figure 2. UV–Vis diffuse reflectance spectra of the organo-functionalized SiO_2-Al_2O_3 mixed oxides and immobilized manganase nanomediator. Legends: SiO_2/Al_2O_3 mixed oxides (A), Si/Al-*pr*-NH-*et*-N=methyl-2-pyridylketone (B), Si/Al-*pr*-NH-*et*-N=methyl-2-pyridylketone-Mn (C).

3.1.3. SEM and TEM study

Scanning electron microscope images of the nanosized SiO_2-Al_2O_3 mixed-oxides and Mn@Si/Al are shown in Fig. 3. It could be seen that the nanoparticles appearance and size of them were similar, demonstrating that the nanoparticles of SiO_2-Al_2O_3 mixed-oxides have good mechanical stability and

they have not been destroyed during the whole modifications. TEM micrograph of the modified mixed–oxides, Fig. 3, shows that the involvement of Mn ions confined onto the organo-functionalized nanosized SiO_2-Al_2O_3 mixed-oxides, are well dispersed (Mn ions did not accumulate and dispersed as Mn nanoparticles) (see Fig. 4)**.**

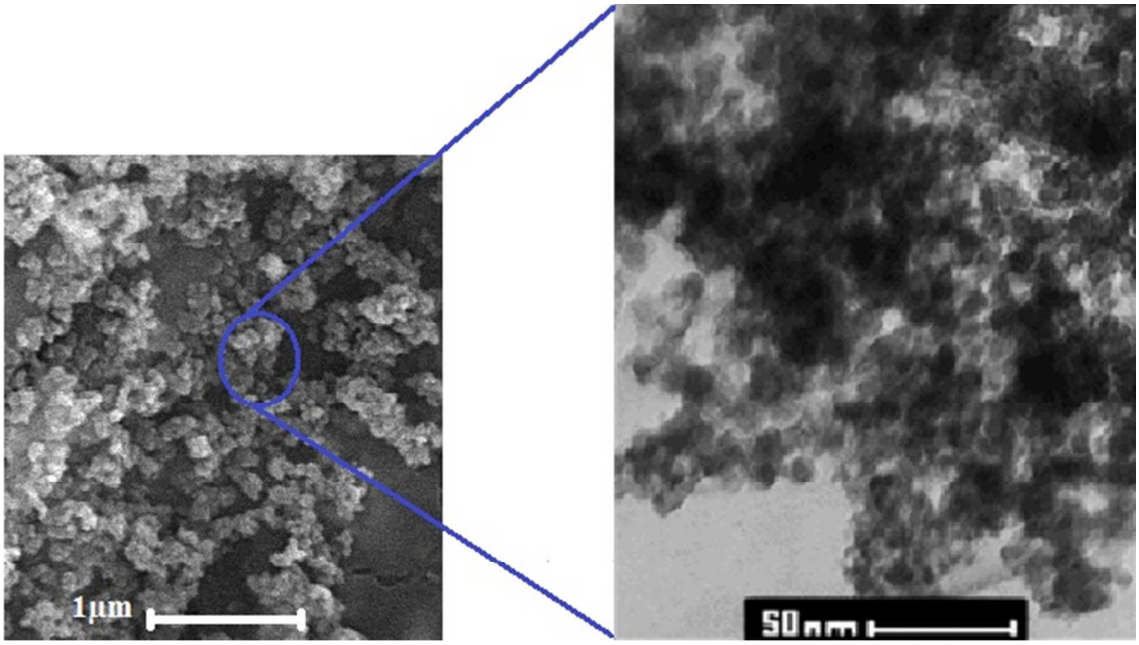

Figure 3. SEM micrographs of Mn@Si/Al (left) and TEM micrograph of Mn@Si/Al (right).

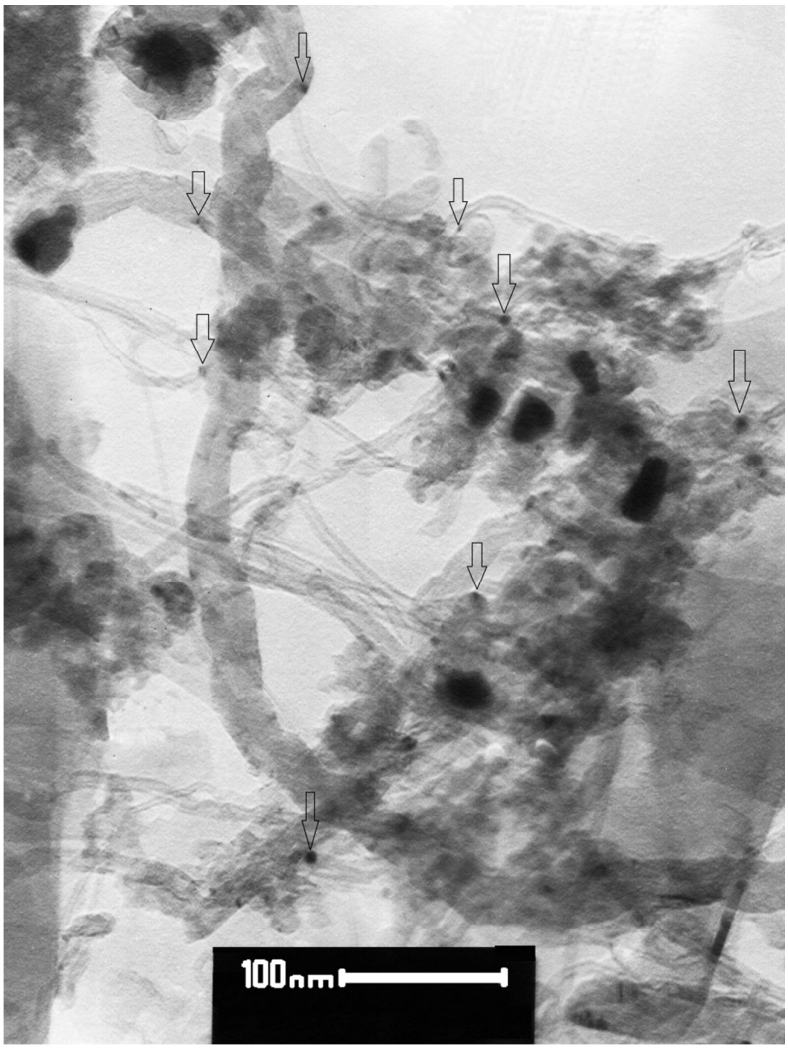

Figure 4. Mn nanoparticles; TEM micrographs of Mn@Si/Al plus carbon nanotubes paste electrode (the dark spots are Mn nanoparticles).

3.1.4. EPR spectroscopy

EPR spectroscopy has been employed to confirm the oxidation state and the chemical environment of Mn species present in the sample. The extreme spin–spin coupling of an even number of unpaired electrons combined with an extremely short relaxation time, makes Mn(III) ions hard to monitor by EPR spectroscopy. For Mn(II) ions with an electron spin S = 5/2, there are five

different ΔM = 1 transitions, where M is the electron spin quantum number. For an isotropic g factor, transitions other than ΔM = +1/2 ↔ -1/2, forcefully depend on the orientation with respect to the magnetic field and are typically not monitored in powder samples. The ΔM = +1/2 ↔ -1/2 transition splits into a sextet by the hyperfine splitting of the Mn nuclear spin I = 5/2. The +1/2, *m* ↔ -1/2, *m* transitions with Δ*m* = 0, where *m* is the nuclear spin quantum number, are allowed transitions that give a sextet spectrum, and the ΔM = 1, Δ*m* = 1 transitions are forbidden transitions that show weak lines between the lines of the sextet.

The X-band EPR spectrum of the immobilized Mn nanoparticles onto the functionalized SiO_2/Al_2O_3 mixed oxides measured at room temperature is indicated in Fig. 5. The EPR spectrum shows that some of the Mn ions are in the other oxidation states, because Mn(III) exhibits no EPR signal. The observed EPR signals, characteristic of Mn(II) / Mn(IV), indicate that, at least, part of the Mn ions are presented in the +2 or +4 oxidation state upon immobilization on the functionalized SiO_2/Al_2O_3 mixed oxides. Thus, next to Mn(III), both Mn(II) and Mn(IV) species must be present, and the observed EPR spectrum must be due to one or both of these species (the reported g values for Mn(IV) are slightly less than 2, whereas those of Mn(II) are slightly above 2).

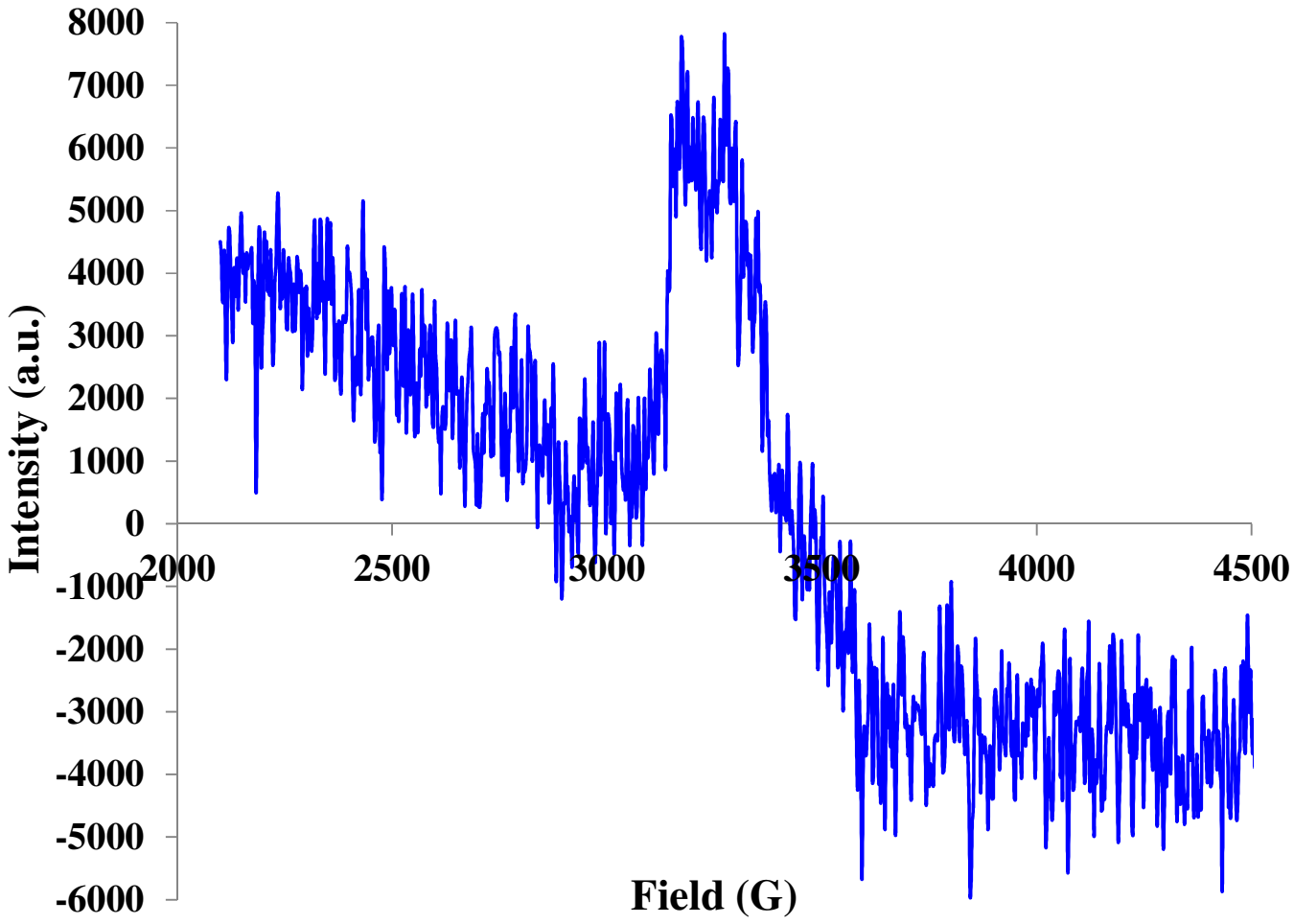

Fig. 5. EPR spectrum of the Mn@Si/Al.

The EPR spectrum appeared to have a broad feature centered around g = 2, with wide wings (Such wings are typical for a distribution of the zero-field splitting parameters, and have been described for Mn(II) in glass environments,[37] or for frozen solutions of Mn(II) phosphate complexes).[38] In fact, the peak broadening and wings are due to dipole-dipole interactions,[39] consequently, they are predominant in the spectra of higher loaded samples (samples containing more than 1.5 wt % Mn).[40]

The EPR spectrum of Mn@Si/Al has a lower intensity in comparison with the other spectra as reported in literature. On the other hand, the inductively coupled plasma optical emission spectroscopy (ICP-OES) analysis of the samples indicates that the nanoadsorbent has a high loading of manganese. This contradiction might be explained by stating that Mn(III) species (expected to be EPR silent under these conditions) probably are the most likely product of the reaction between Mn(II) and Si/Al-*pr*-NH-*et*-N=methyl-2-pyridylketone.

Therefore, Mn(III) is the main oxidation state which immobilized on the functionalized SiO_2/Al_2O_3 mixed oxides and probably MO was mainly captured by Mn(III). It is believed that during the immobilization of Mn(II) over the modified SiO_2/Al_2O_3 under air condition (in the presence of an atmospheric oxygen) oxidation state of Mn(II) was easily oxidized and began to prefer the Mn(III) state (In fact, oxidation of Mn(II) gives a stable cation; Mn(III)). The EPR peak broadening of the Mn@Si/Al could be due to the presence of Mn(II) and Mn(IV) in its structure (g = 1.95). Microcrystalline nano-catalysts often yield characteristic EPR spectra with features distinctly different from those observed for magnetically isolated ions. The detailed features of the resonances depend strongly on shape, size distributions and on the magnetic properties of the particles. Consequently, with regard to the EPR spectrum and TEM photo, the broad feature around g_{av} = 2.03 is probably characteristic of super paramagnetic relaxation as it concerned with the magnetic moment of the whole

particle and either may be due to the highly dispersed of Mn species on the nano-adsorbent (Fig. 5).

3.1.5. XPS

The XP spectroscopic analysis of the heterogeneous catalyst was used to study for the characterization of oxidation state of the immobilized Mn-nanoparticles on the surface of modified-SiO_2/Al_2O_3. This technique has previously been shown to provide valuable information regarding the chemical state of the catalytically active sites in different catalysts.[41] The XPS spectrum of Mn catalyst produced a Mn $2p_{3/2}$ and a Mn $2p_{1/2}$ peak at 643.01 and 654.61 eV, respectively, and are depicted in Fig. 6. However, there is two satellite peaks at 647.5 and 659.4 eV beside the main peak of Mn $2p_{3/2}$ and Mn $2p_{1/2}$ in Mn@Si/Al. These results indicated that most of the Mn ions on the surface of the support were in +3 oxidation state (due to the binding energy (BE) 643.01 eV of Mn $2p_{3/2}$ which is attributed to Mn(III) state of the nanoparticles).

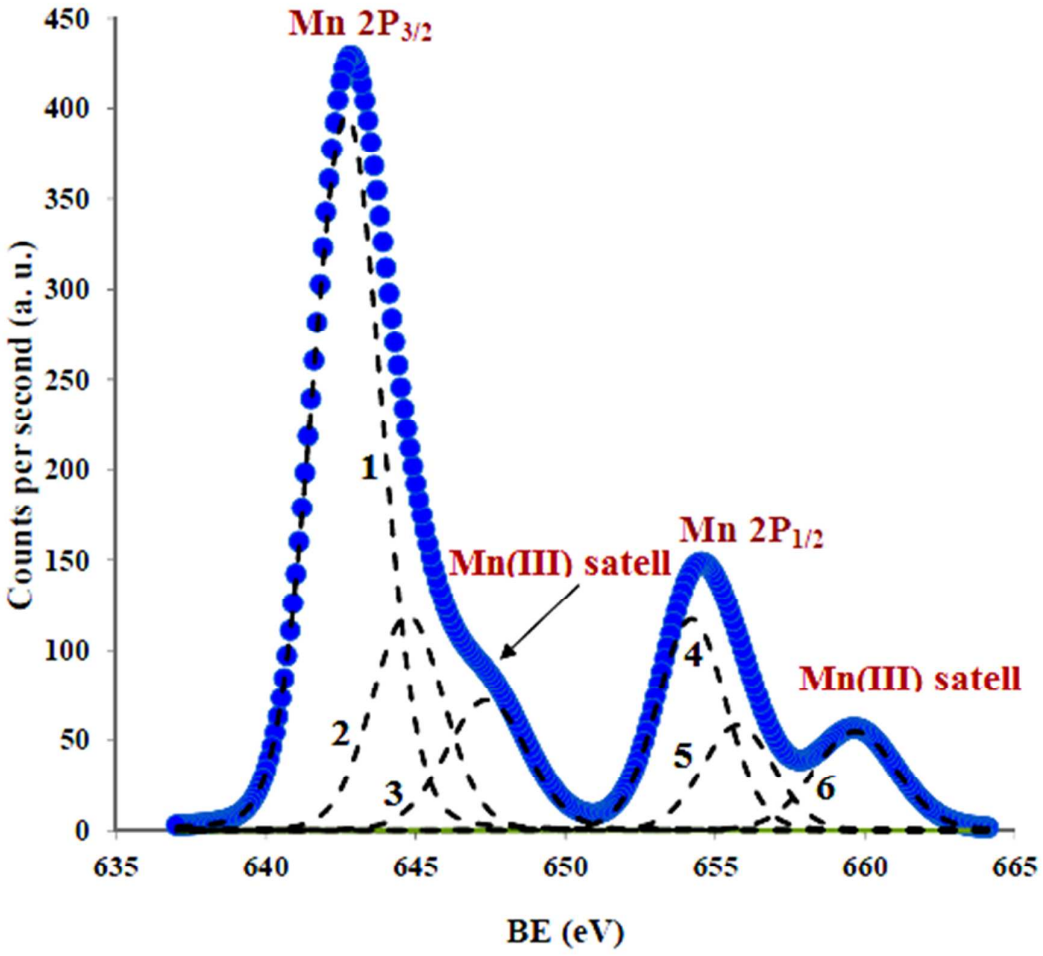

Figure 6. XP spectroscopy of the Mn@Si/Al. The Mn $2p_{3/2}$ component is fit by multiplet peaks labeled 1, 2 and 3, with peak 3 corresponding to the shake-up satellite. The Mn $2p_{1/2}$ component is fit by two peaks and a satellite peak.[42]

3.2. Adsorption study

Preliminary experiments showed that the nano-sized SiO_2–Al_2O_3 has the low capacity to remove MO dye from the wastewater. So in this work various processes of pretreatment are designed on the nano-sized SiO_2–Al_2O_3 with the aim of enhancing the MO adsorption capacity by altering the chemical

modification to give more active sites and/or by obtaining suitable physical structure of the available functional groups.

3.2.1. Effect of initial pH on methyl orange ion adsorption

The effect of pH plays an important role on the active sites of nano-adsorbent as well as the dye speciation during the adsorption reaction.[1-20] In order to evaluate the influence of pH on the adsorption capacity of the Si/Al and Mn@Si/Al, experiments were carried out at initial concentration of 105 mg L^{-1} and in the pH range 1.0–13.0 (Fig. 7).

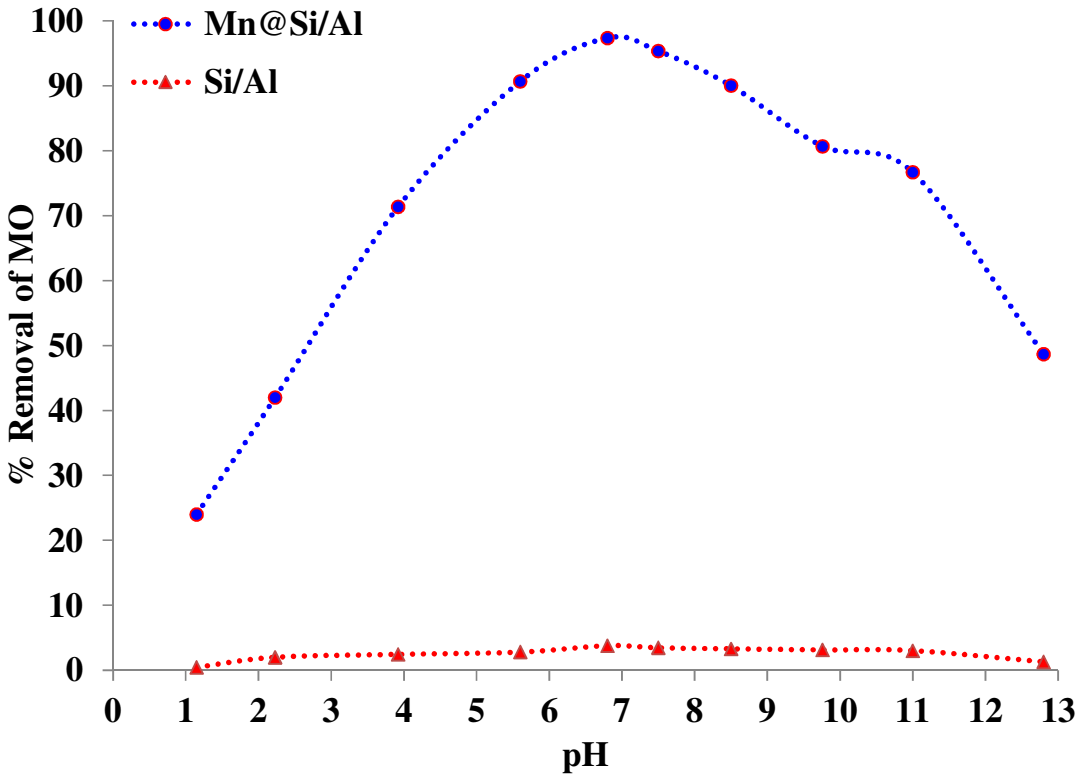

Figure 7. Effect of pH on MO ions sorption from aqueous solution.

As shown in Fig. 7, the modified Si/Al nano-sized mixed oxides with organometallic groups indicates higher MO capturing capacity than the unmodified Si/Al at various pH values. The results indicate that there is a significant influence of pH on the adsorption of MO onto the Mn@Si/Al. Similar observation was published in the literature onto the different adsorbents. [10-30] As the initial pH increased to 6.8 sorption capacity increased to more than 97.3 % and decreased at the initial pH values above 6.5 (>48.6 %). The lowest MO sorption capacity of Mn@Si/Al (48.6 %) was found at an initial solution pHs of 13.0, which may be due to partial dissolution of the immobilized Mn ions at this solution pH (data not published).

At acidic pH protons can be picked up on one of the nitrogens in nitrogen–nitrogen double bond, which can generate a reddish color of MO dye solution, that is, MO was protonated and hence the electrostatic repulsion interaction between protonated MO and positively charged Mn@Si/Al active sites result a decline in the percentage of adsorption (the dissociation constant pKa for MO is 3.46, so MO molecules were predominantly present as monovalent anions at this equilibrium pH). However, decreasing MO adsorption in basic pH may be attributed to the competition of OH^- with MO ions for adsorption sites on the Mn@Si/Al (the active sites; Mn(III) ions, are closely associated with hydroxyl ions OH^-, that is, restricted the approach of MO ions, as a result of the repulsive force) and therefore fewer groups are available for MO to bind with. Therefore, the possible mechanism of MO

adsorption may be considered as the strong electrostatic interaction between the positive adsorption active site of the adsorbent and the negatively charged MO (Scheme 3). This pH-dependent trend has also been observed for the adsorption of similar anionic dyes onto TiO_2,[43] activated carbon modified with Y(III) ions [44] and Copper(II) Complex of dithiocarbamate-Modified Starch, [45] confirming the interaction of the anionic dyes with metal centers, which direct the adsorption process.

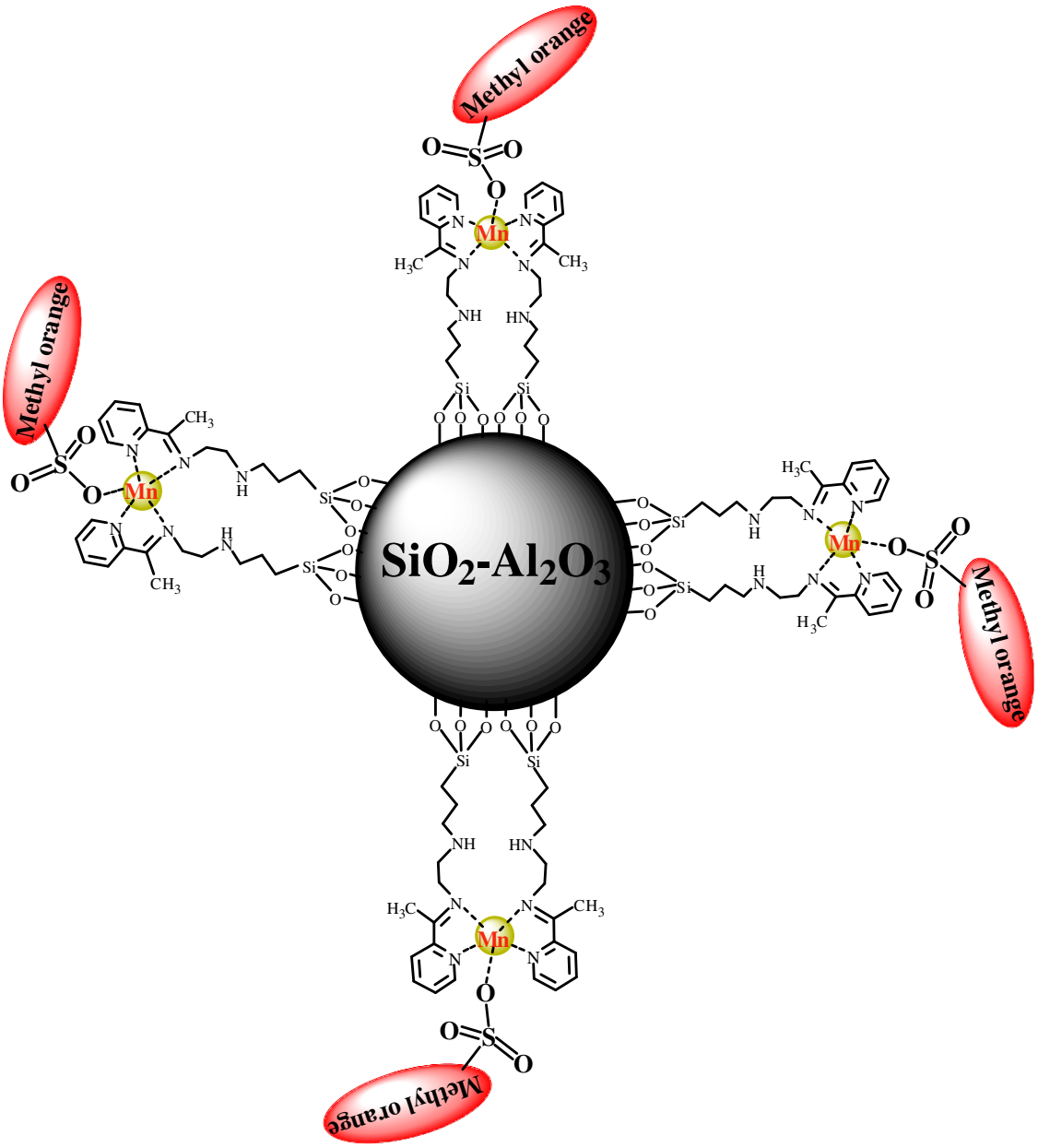

Scheme 3. The proposal mechanism for heterogenization of MO by Mn@Si/Al.

For further study the oxidation state of the immobilized Mn ions at different pH, ESR spectra of the Mn@Si/Al at pH 2.0 measured (Fig. 8) and compared with those recorded at pH 7.0 (Fig. 5). Among the methods used in

this study [Fourier transform infrared (FTIR), diffuse reflectance UV/Vis (DRS) and electron paramagnetic resonance (EPR)], EPR was found to be sensitive to the oxidation state of the manganese atom at different pH. The ESR spectra of the Mn@Si/Al at pH lower than 4 show similar features as that of Mn@Si/Al at pH higher than 4.0. But the intensity of ESR spectra of Mn@Si/Al at pH > 4.0 is less than that recorded at pH < 4.0. The intensity of ESR spectrum of Mn@Si/Al at pH 2.0 shows high intensity with a *g* value of about 2 than those prepared at pH >4.0, which was consistent with Mn(II) (g = 2.0) in the environment of distorted octahedral symmetry. Therefore, the sample at pH>4.0, there might be more oxidation of Mn(II) to Mn(III). Indeed, Mn(III) sites are also on the Mn@Si/Al, as they are more inclined to get into the framework than Mn(II).[46] In order to introduce more number of Mn(III) on the Mn@Si/Al, conversion of Mn(II) to Mn(III) is required. Since this oxidation can be carried out by dissolved O_2, pH higher than 4 might be more effective than pH 2.0 or 3.0 to dissolve more oxygen and to increase oxidation. However, this results revealed that better heterogenization of Mn(II) on the active sites of Schiff base ligands can be obtained at pH lower than 4.0. Thus, increasing the concentration of Mn(III) on the Mn@Si/Al is feasible if the experimental pH is raised to 4.0. All the above experiments clearly reveal that the acidity of the solution influences the electronic structure of the immobilized Mn nanoparticle.

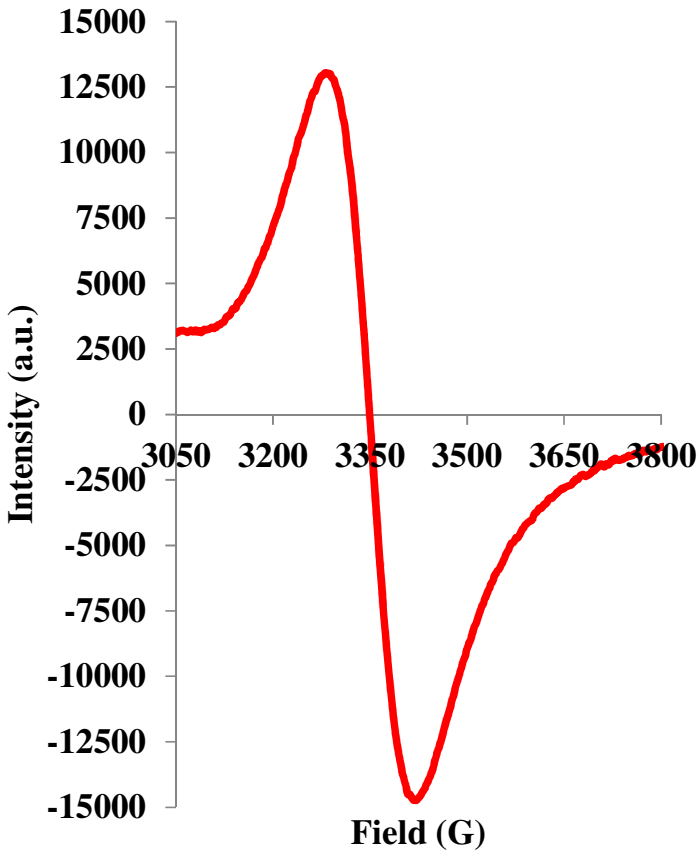

Fig. 8. EPR spectrum of the Mn@Si/Al at pH 2.0.

3.2.2. Effect of adsorbent dosage

The adsorbent dosage is one of the important factors as it presented the capacity of the adsorbent for a given initial amount of the adsorbate. To determine the correlation of MO sorption on adsorbent dosage, various dosages (0.010-1.00 g) of Mn@Si/Al, at a controlled temperature of 25 ± 1°C, was added into 10 mL of 105.0 mg L^{-1} MO solution without any changes on the solution pH (Fig. 9). The relation between the adsorbent dosage and removal percentage of MO by the Mn@Si/Al is shown in Fig. 9, from which it can be

seen that the removal percentage of MO increased with increasing the adsorbent dosage, probably could be due to an increase in the number of adsorption sites. As the adsorbent dosage increased from 0.010 to 0.15 g, the removal efficiency of MO ions increased significantly from 46. 0% to 99.3%.

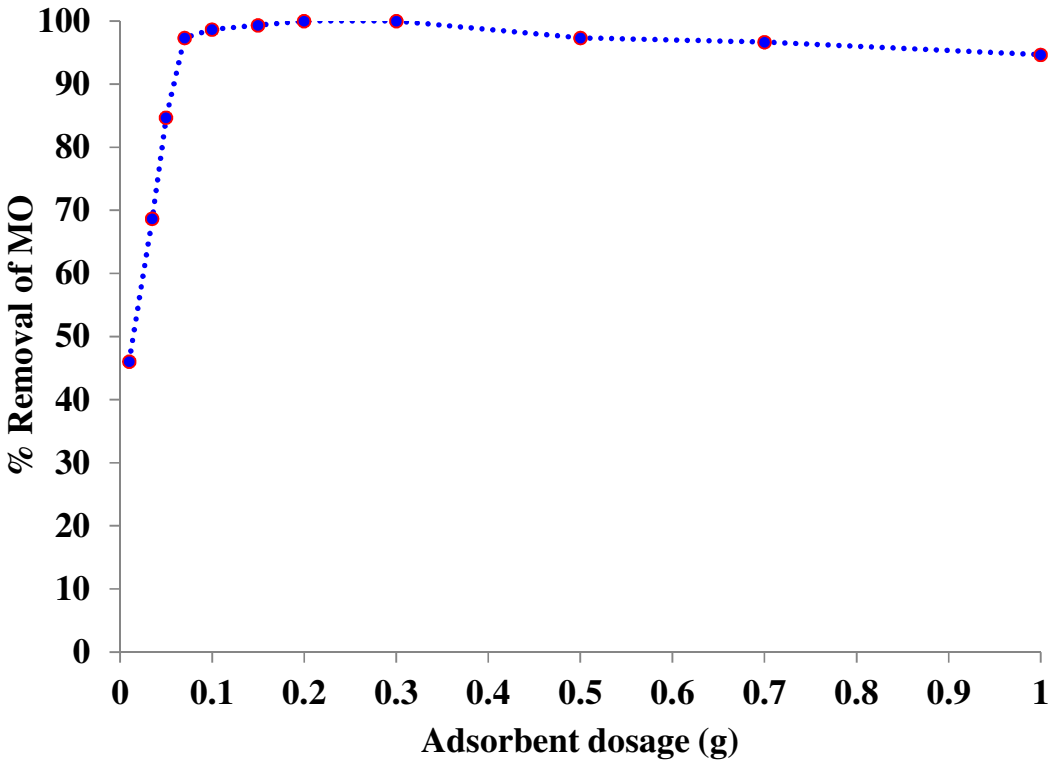

Figure 9. Effect of adsorbent dosage on the sorption of Mo ions by the Mn@Si/Al from aqueous solution.

However, the higher adsorbent dose results in a lower removal capacity of Mn@Si/Al (94.6%). It is believed that at the low adsorbent dosage the dispersion of Mn@Si/Al nanoparticles in aqueous solution is better, that is, all of the active sites on the adsorbent surface are entirely uncovered which could

accelerate the approachability of MO molecules to a large number of the adsorbent active sites. Thus, the adsorption on the active sites is saturated quickly, performing a high removal capacity. On the other hand, at higher adsorbent dosage, the accessibility of adsorbent active sites with higher energy decrease and a larger fraction of the active sites with lower energy becoming occupied; leading to a decrease in adsorption capacity. Furthermore, increasing adsorbent dosage enhances the chance of collision between adsorbent nanoparticles and hence creates particle aggregation, inducing a decline in the total surface area and an increase in diffusion path length, which both result in a decrease in the amount of removal capacity of MO from aqueous solution. Therefore, 0.07 g of adsorbent dosage was chosen as the optimal dosage for the rest of the study.

3.2.3. Effect of the initial concentration on the uptake

The adsorption results obtained for Si/Al and Mn@Si/Al upon varying initial MO ion concentrations (0.75–1000 mg L−1) are illustrated in Fig. 10, where it can be seen that Mn@Si/Al was demonstrated to be the most efficient in that more than 97.0% of MO was removed after 15 min, whereas only 4.2% of MO was removed by Si/Al. The Si/Al utilized in this investigation is a nano-sized mixed oxides and it shows low efficiency in removal of MO, but provided good suspensibility and dispersibility for organometallic groups, when

removing MO from aqueous solution and it improved the reactivity of Mn@Si/Al.

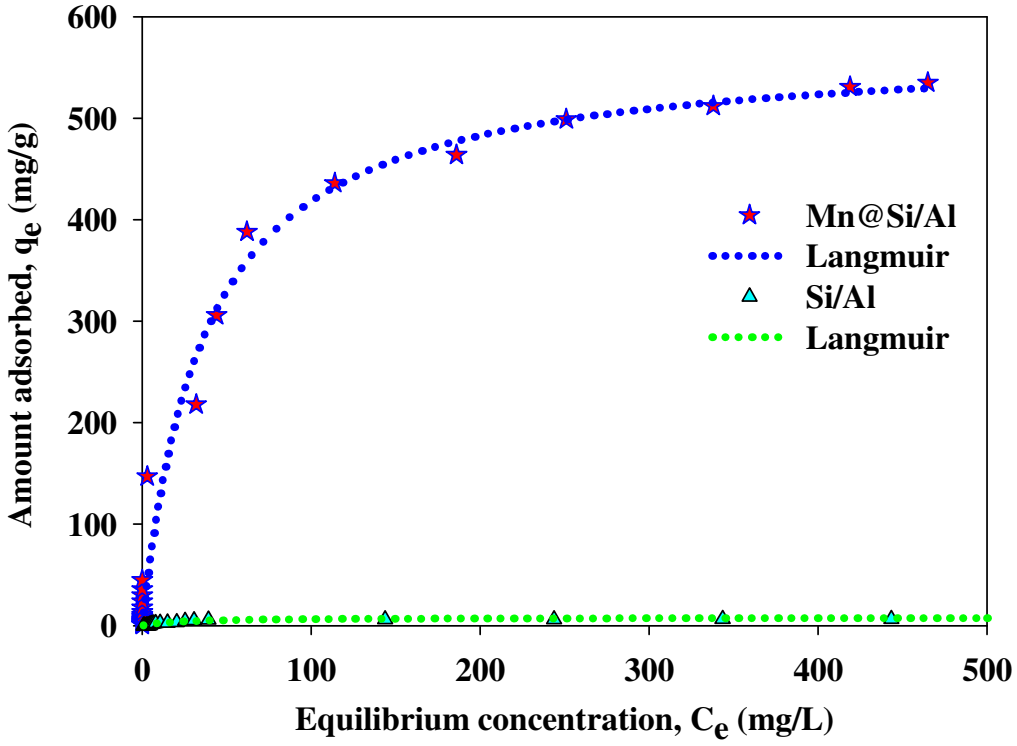

Figure 10. Equilibrium absorption of MO by the Si/Al and Mn@Si/Al at 25 ◦C. Dash line represents the fitting curve using the Langmuir adsorption model.

When the initial MO concentrations were increased in the presence of Mn@Si/Al, the removal efficiency of the dye reached to 98.0 % and 53.5 % for 150 and 1000 mg L^{-1} initial dye concentration, respectively. The relative increase in the loading capacity of sorbent with increasing MO concentrations is probably due to the interaction between the dye and adsorbent which provides the vital driving force to defeat the resistance to the mass transfer of MO ions

between the aqueous solution and Mn@Si/Al. The observed enhancement of MO uptake with increasing the initial dye ions concentration could be due to an increase in electrostatic interactions (relative to covalent interactions), which involves active sites of progressively lower affinity for MO up to saturation point. On the other hand, the higher removal efficiency of Mn@Si/Al at low MO initial concentration could be related to the high ratio of initial mole numbers of MO to the available active sites on the surface area; therefore, the fractional adsorption is dependent on the initial concentration.

3.2.4. Adsorption isotherms

Equilibrium adsorption isotherms are known to be very important when they come to understanding adsorption mechanisms. Thus, the experimental adsorption equilibrium data of MO dye on Mn@Si/Al were fitted by applying the Langmuir and Freundlich isotherm models, which are typically used for aqueous-phase adsorption (Table 3).[1-30] These adsorption models give a representation of the adsorption equilibrium between an adsorbate in solution and the surface active sites of the adsorbent. The Langmuir and Freundlich adsorption isotherms can be expressed by eqs. 2 and 3, respectively.

$$q_e = q_m K_L C_e / 1 + K_L C_e \quad (2)$$

$$q_e = K_F C_e^{1/n} \quad (3)$$

where q_e (mg g^{-1}) is the specific equilibrium amount of adsorbate, C_e (mg L^{-1}) is the equilibrium concentration of adsorbate, q_m is the maximal adsorption

capacity, K_L is the Langmuir isotherm constant (L mg $^{-1}$), K_F is the Freundlich isotherm constant (mg g^{-1} (mg $L^{-1})^n$) and n which is an indicator of the adsorption effectiveness. The constant n gives an idea of the degree of heterogeneity in the distribution of energetic centers and is related to the magnitude of the adsorption driving force. High n values therefore indicate a relatively uniform surface, whereas low values mean high adsorption at low solution concentrations. Furthermore, low n values indicate the existence of a high proportion of high-energy active sites.

Table 3. Fitting of the parameters of the experimental results to the Langmuir and Freundlich equation parameters.

System	q_m (mg g^{-1})	K_L (L mg^{-1})	K_F (mg g^{-1} (mg $L^{-1})^n$)	n	R^2	Sorption model
Mn@Si/Al						
	571.2	2.73× 10^{-2}			0.9927	Langmuir
			0.448	0.294	0.6927	Freundlich

The Langmuir equation relates the coverage of molecules on a solid surface to concentration of a medium above the solid surface at a fixed temperature and adsorption is limited to monolayer coverage, and intermolecular forces decrease with the distance from the adsorption surface, whereas the Freundlich model supposes that the adsorption surface is heterogeneous, that interaction between adsorbed molecules can occur, and that multilayer adsorption is possible. The Langmuir and Freundlich adsorption isotherms exhibit an approximately linear relationship for Mn@Si/Al. The data obtained from the Mn@Si/Al revealed that Langmuir isotherm model correlated

better (R^2>0.9827) than Freundlich isotherm (Table 3 and Fig 10), using the experimental data for the adsorption equilibrium of MO ions by the modified SiO_2-Al_2O_3 mixed oxides, thereby it is realistic to infer that the adsorption active sites on the modified Si/Al are not mostly energetically heterogeneous (non-uniform surface), and this is a major aspect in this model. Likewise, the maximum adsorption capacity (*qm*) for Mn@Si/Al (571.2 mg g^{-1}), as obtained using the Langmuir isotherm, was much higher than the values found for the most other adsorbents reported in the literature,[3-30] thereby also suggesting that there is a high thermodynamic stability for MO heterogenization at the active sites of Mn@Si/Al (Table 3).

3.2.5. Adsorption kinetics

The effect of shaking time (0-240 min) on the adsorption of MO (150 mg L^{-1}) onto Mn@Si/Al (0.07 g), in a solution with pH 6.5 at 25^{o}C was shown in Fig. 11, from which it can be seen that the amount of adsorption increases with increasing the contact time. Studies of the adsorption kinetics of MO removal revealed that the majority of dye (98.0 %) was removed within the first 0-15 min contact with the modified nano-adsorbent. Percentage of maximum adsorption was 99.8 % at 240 min. Indeed, the fast adsorption during the initial stage is probably due to the high concentration gradient between the adsorbate in solution and that on the adsorbent as there are a high number of vacant sites available during this period, while the obtained plateau after 15 min relates to a

slow rate of adsorption which could be due to an agglomeration of MO molecules on the Mn@Si/Al active sites. Therefore, in order to optimize the adsorption process, the adsorption isotherms for the remaining of initial concentrations were obtained for a contact time of 15 min.

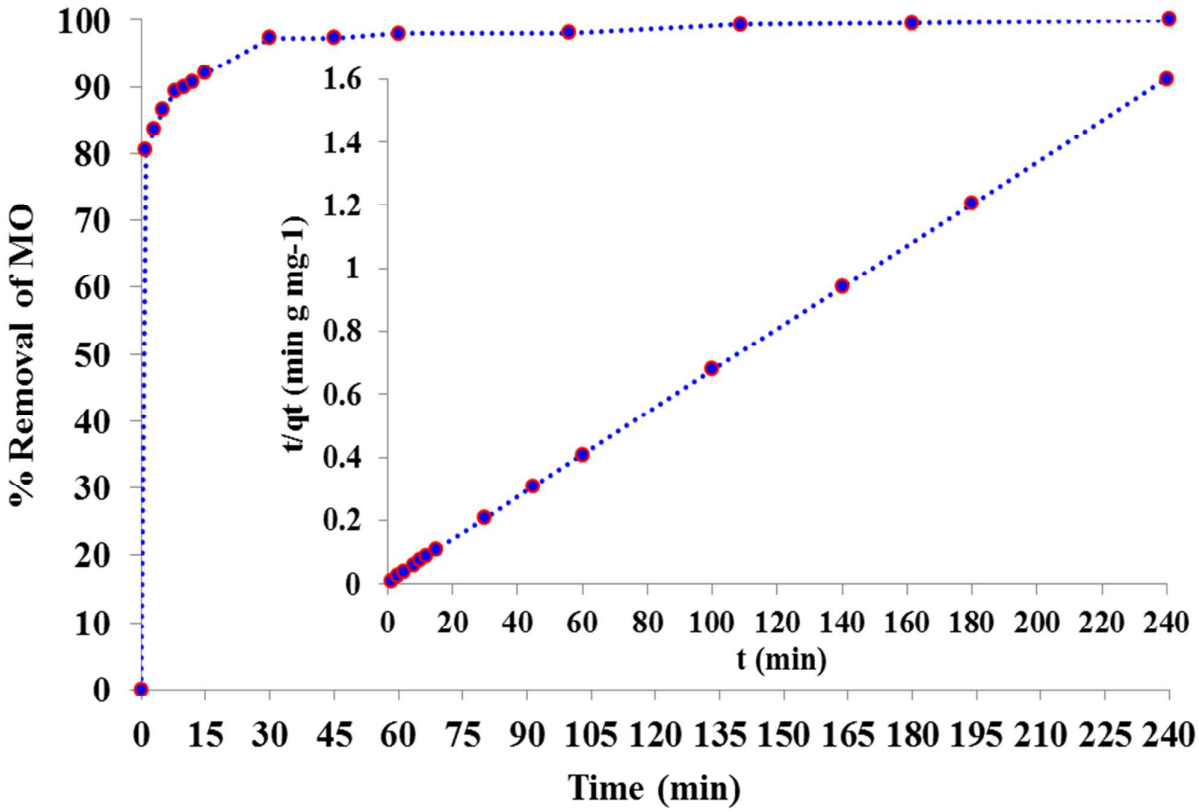

Figure 11. The adsorption kinetics of the Mn@Si/Al for MO at room temperature. The inset shows pseudo-second order plot for the adsorption.

In order to determine and interpret the mechanisms of MO adsorption processes and the main parameters governing sorption kinetics, empirically obtained kinetic sorption data were fitted to the pseudo-first-order, pseudo-second-order, and intra-particle diffusion models shown in eqs 4, 5, and 6, respectively. Each of these models has been widely used to describe metal and

organic sorption on several sorbents.[1-,2] From the linear form of these three models, equations can be written as follows:

Pseudo-first-order equation: $q_t = q_e[1-exp(-k_1t)]$ (4)

Pseudo-second-order equation: $q_t = k_2q_e^2t/1 + k_2q_et$ (5)

Intra-particle diffusion equation: $q_t = k_{int}t^{1/2}$ (6)

The initial adsorption rate (h) can be determined from k_2 and q_e values using

$$h = k_2q^2_e \quad (7)$$

Where k_1, k_2 and k_{int} are the adsorption rate constants of first, second order kinetic and intra-particle diffusion models, in min^{-1}, L (mg min)$^{-1}$ and mg g^{-1} $min^{-1/2}$, respectively; q_e and q_t in mg g^{-1}, are equilibrium adsorption uptake (at time $t = \infty$) and adsorption uptake (at time t), respectively.

Table 4. Kinetic parameters for the adsorption of MO by Mn@Si/Al.

Pseudo first order constants	Pseudo second order constants	Intra-particle diffusion constants
k_1 (min^{-1}) = 0.623	k_2(g/(mg min)) = 0.0065	K_{int} (mg/(g $min^{1/2}$)) = 1.7743
q_1 (mg/g) = 144.9	q_2 (mg/g) = 149.2	R^2 = 0.7486
R^2 = 0.8563	h (mg/(g min)) =144.9	
	R^2 = 1	

The calculated kinetics parameters for adsorption of MO dye ions onto the Mn@Si/Al, at initial concentration of 150 mg g^{-1} are presented in Table 4, where it can be seen that the pseudo-second-order equation appeared to be the best-fitting model than those for the other two equations (the correlation coefficient is extremely high for the pseudo-second-order equation of Mn@Si/Al; R^2> 0.999). The value of $q_{e,cal}$ also appeared to be very close to the experimentally observed value of $q_{e,exp}$. The plot of linear form of the pseudo-

second-order for the adsorption of MO ions was shown in the inset of Fig 11. Similar results have been reported about the adsorption of dyes onto the different adsorbents in the literature.[1-10]

This consistency of the experimental data with the pseudo-second-order kinetic model indicates that the rate limiting step for the adsorption of MO ions on the organometallic-functionalized SiO_2-Al_2O_3 mixed oxides is chemical adsorption (scheme 3). As a result, the adsorption of the MO dye onto the nano adsorbent may be considered to involve two processes with initial adsorption rate of 144.9 mg $(g\ min)^{-1}$ over Mn@Si/Al. Although this adsorption rate is related to the content and type of active adsorption site on the matrix of adsorbent, Mn(III) sites are the main reactive groups for the removal of MO ions from aqueous solution. More advantage of the pseudo-second-order model is that it predicts the behavior over the whole range of the adsorption process.

3.2.6. Effect of the temperature on the uptake

Furthermore, the equilibrium adsorption capacity of MO onto the favored adsorbent, Mn@Si/Al, were studied at different range of temperatures of 15, 25, 40, 60 and 80 ^{o}C in pH = 6.5 (Fig. 12). The increase in the temperature of solutions of MO from 15 to 80 ^{o}C leads to increase in the adsorption capacity of Mn@Si/Al, thereby indicating that adsorption of the dye onto active sites of Mn@Si/Al are endothermic, possibly due to availability of more such active sites and the enlargement and activation of the adsorbent surface at higher temperatures. It could also be due to an increased mobility of MO dye ions from

the bulk solution towards the adsorbent surface, thereby enhancing the accessibility to the adsorbent active sites.

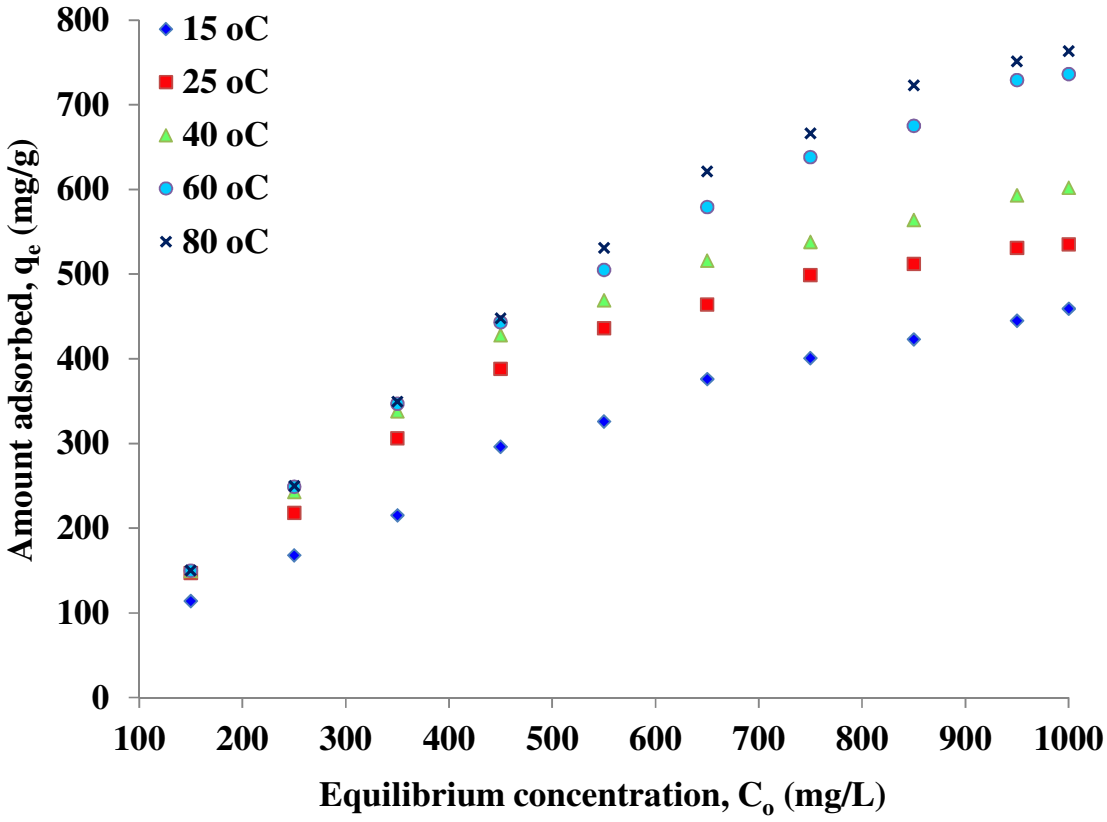

Figure 12. Effect of temperature on the adsorption of MO by the Mn@Si/Al at deferent initial concentrations.

Towards a better understanding of the effect of rising temperature on the adsorption of the dye ions onto Mn@Si/Al, three basic thermodynamic parameters were studied: the Gibbs free energy of adsorption (ΔG°), the enthalpy change (ΔH°), and the entropy change (ΔS°).

The thermodynamic parameters ΔG°, ΔS° and ΔH° for this adsorption process were determined by using following equations.[60]

$$\Delta G = -RT \ln K \quad (8)$$

where K is the thermodynamic equilibrium constant. The values of K can be determined by plotting $\ln(q_e/C_e)$ against qe and extrapolating to zero, where q_e is the adsorbed MO ions concentration at equilibrium and C_e is the equilibrium concentration of MO ions in solution. The effect of temperature on thermodynamic constant was determined by Eq. (9)

$$d\ln K/dt = \Delta H^o/RT^2 \quad (9)$$

The ΔH° and ΔS° values were calculated from slope and intercept of the linear plot, of lnK vs 1/T as shown in Fig. 13.

$$\ln K = \Delta S^o/R - \Delta H^o/RT \quad (10)$$

and Gibbs free energy is given by Eq. (11), where ΔG° is the free energy change (J/mol); R and T is the universal constant (8.314 J/mol K) the absolute temperature (K), respectively.

$$\Delta G^o = \Delta H^o - T\Delta S^o \quad (11)$$

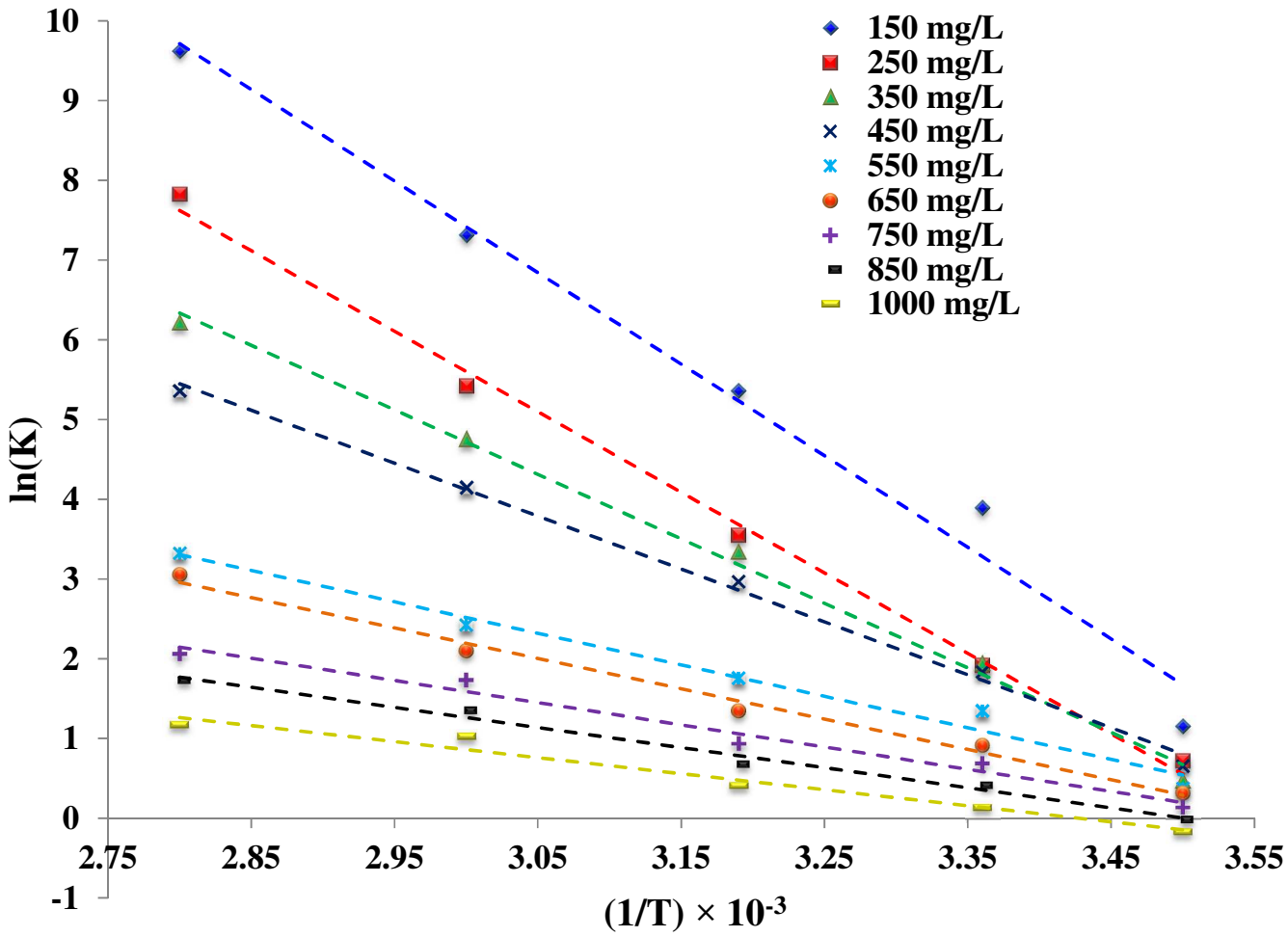

Figure 13. Plot of lnK vs. 1/T for the MO adsorption onto Mn@ Si/Al.

Table 5. Thermodynamic parameters for the adsorption of MO onto Mn@Si/Al as a function of temperature.

Initial MO concn.	ΔH^o	ΔS^o	ΔG^o/kJ/·mol				
mg/L	(J/mol)	(J/(mol K))	288	298	313	333	353
150	95.45	348.11	-100.16	-103.64	-108.86	-115.82	-122.79
250	80.00	298.58	-85.911	-88.896	-93.375	-99.347	-105.31
350	67.25	240.98	-69.334	-71.744	-75.359	-80.179	-84.998
450	55.18	199.84	-57.498	-59.497	-62.494	-66.491	-70.488
550	32.84	119.45	-34.368	-35.563	-37.355	-39.744	-42.133
650	31.66	113.26	-32.587	-33.719	-35.418	-37.683	-39.949
750	23.15	82.66	-23.782	-24.609	-25.849	-27.502	-29.155
850	20.93	73.30	-21.089	-21.822	-22.921	-24.387	-25.853
1000	16.73	57.33	-16.494	-17.067	-17.927	-19.074	-20.220

The corresponding values of thermodynamic parameters are presented in Table 5. This shows that ΔH^o and ΔS^o are positive for all the experiments and ΔG^o is negative in all systems. The positive values of ΔH^o revealed that the adsorption process was endothermic in nature; thus removal of MO increases with increasing temperature. The positive value of $\Delta S°$ revealed an increase in randomness and an increase in the degrees of freedom at the Mn@Si/Al-solution interface during the immobilization of the MO dye ions on the active sites of the adsorbent, where methyl orange is a bulk molecule in comparison with H_2O; so some water molecules could be desorbed during the adsorption of a methyl orange molecule. This process led to a partial liberation of the solvated MO ions from solvent molecules before adsorption (liberation of water molecules from solvated-MO), thereby enabling commonness of randomness and spontaneity in the system.[1,2] The necessity of a large amount of heat to remove the MO dye ions from the solution makes the sorption process endothermic. The positive $\Delta S°$ (disorder of the system) was observed on Mn@Si/Al, which indicates that MO ion lose most of their water of solvation. This is also supported by the positive $\Delta H°$ value of MO sorption onto

Mn@Si/Al. The positive value of the standard enthalpy change for MO ions sorption indicates endodermic nature of adsorption. It was also observed that with increase in temperature the value of ΔG decreases, which indicated that sorption process was spontaneous and thermodynamically favorable by an increase in temperature (Table 5). In fact, the value of ΔG^o for physisorption is in the range $-20 > \Delta G^o < 0$ kJ/mol, but chemisorption is between $-400 > \Delta G^o < -80$ kJ/ mol.[47] The calculated ΔG^o values based on Eq. (14) were more than -40 kJ/mol for most of the cases (Table 5) Therefore, the ΔG^o values suggested that adsorption of MO ions onto the Mn@Si/Al was a chemisorption process, as the adsorption mechanism was proposed in scheme 3.

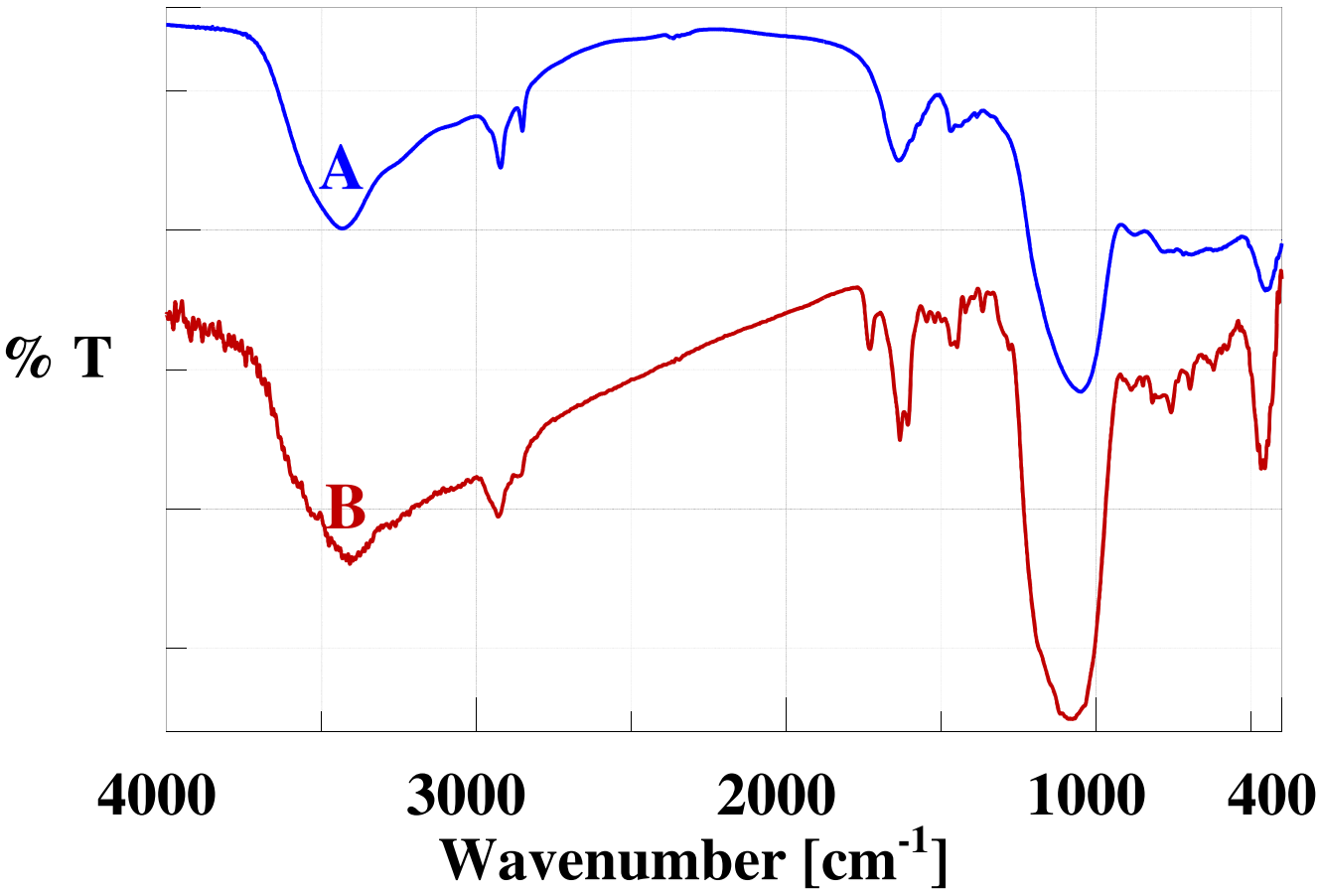

Figure 14. FTIR spectra of the Mn@Si/Al before and after adsorption of MO from aqueous solution. Legends: Mn@Si/Al (A), Mn@Si/Al after MO adsorption (B).

To prove the proposed mechanism in scheme 3, FT-IR of Mn@Si/Al and MO-loaded Mn@Si/Al samples, before and after the adsorption process, were recorded in the range 4000–400 cm^{-1} (Fig. 14). FTIR is often used to study the active sites of the adsorbents and to identify the interactions of those groups responsible for the dye adsorption. The adsorption ability of the Mn@Si/Al for

MO dye ions from aqueous solution is resulted from the strong interaction of active sites of immobilized Mn nanoparticles towards the dye. In the equilibrated sample of the Mn@Si/Al with MO solution, extra bands at 1729, 1606, 1447, 1421, 620 and 577 cm^{-1} were observed showing the presence of MO anchored to the active sites of the modified nano-adsorbent. The peak at 1729 cm^{-1} is enhanced in the Mn@Si/Al-MO. This may belong to coordinated sulfonate group, and generally appears when the bond between the metal and oxygen is strong (Mn–O–SO_2–R, scheme 3).[48] The modes of MO ions coordination with the immobilized Mn(III) is evidenced through O atoms of the sulfonate group by appearing a new band around 577 cm^{-1} (Fig. 14). Indeed, the new absorption peaks observed in the range of 560 to 660cm^{-1} was the characteristic absorption peaks of "Metal–O" bond, which demonstrating the existence of the Mn–O bond (Mn–O–SO_2–R, scheme 3).[49] Also, the kinetics results proved that the adsorption obeys a pseudo second-order kinetics model that indicates that the adsorption involves chemisorption.

In order to clarify further into the mechanistic aspects of the MO adsorption onto Mn@Si/Al, desorption study was investigated. The use of water and

ethanol solutions for the MO desorption is ineffective even after 48 h. Very low desorption (do not exceed 7% of the presorbed amount) with these solutions suggested that metal-dye complexes were formed on Mn@Si/A. The high basic solution (above 0.01 mol L^{-1}) did help to breaking the chelating interaction, in which the hydroxyls group replaced the MO to bind the Mn@Si/A.

4. Conclusion

This work shows that mixed oxides modified with Mn nanoparticles could find applications as adsorbent for the removal of hazardous dye ions from aqueous solutions. The synthesized materials were verified by TEM, SEM, EPR, XPS, ICP, BET, UV-vis and FTIR analysis. Several adsorption conditions such as initial dye concentration, contact time, adsorbent dosage and pH on the adsorption capacity of MO will influence the dye adsorption. The kinetic data indicates that the pseudo-second order kinetic model was found to be well suited and provide high degree of correlation with the experimental data for the adsorption process of MO on Mn@Si/Al. The immobilization of Mn nanoparticle produces positive charge on the surface (Mn(III)), which will provide a strong attraction to negatively charged MO ions. Adsorption of MO dye on Mn@Si/Al is an endothermic process. The strong chemical binding

between dye and active sites of the nano-adsorbent results in much less desorption of MO from the solid adsorbent surface.

Acknowledgment

Thanks are due to the Iranian Nanotechnology Initiative for supporting of this work.

References

[1] L. Zhou, C. Gao, W. Xu, *ACS Appl. Mater. Interfaces* 2010, **2**, 1483

[2] T. Robinson, G. McMullan, R. Marchant, P. Nigam. *Bioresource Technology* 2001, 77,247.

[3] M. Arshadia, F. Salimi Vahid, J.W.L. Salvacion, M. Soleymanzadeh, *Applied Surface Science*. 2013, **280**, 726.

[4] H.Y. Zhu, R. Jiang, L. Xiao, G.M. Zeng, *Bioresour. Technol.* 2010, **101** 5063.

[5] J.H. Huang, K.L. Huang, S.Q. Liu, A.T. Wang, C. Yan, *Colloid Surf. A* 2008, **330**, 55.

[6] P. Zhang, Q. An, J. Guo, C.C. Wang, *J. Colloid Interface Sci*. 2013, **389** 10.

[7] W. Cheah, S. Hosseini, M.A. Khan, T.G. Chuah, T.S.Y. Choong, *Chem. Eng. J*. 2013, **215–216**, 747.

[8] Z.M. Ni, S.J. Xia, L.G. Wang, F.F. Xing, G.X. Pan, *J. Colloid Interface Sci*. 2007, **316**, 284.

[9] J. Ma, F. Yu, L. Zhou, L. Jin, M.X. Yang, J.S. Luan, Y.H. Tang, H.B. Fan, Z.W. Yuan,J.H. Chen, *ACS Appl. Mater. Interfaces*, 2012, **4**, 5749.

[10] M.R. Samarghandi, M. Hadi, S. Moayedi, F.B. Askari, *Iran. J. Environ. Health Sci. Eng*. 2009, **6**, 285–294.

[11] Y.J. Yao, B. He, F.F. Xu, X.F. *Chen, Chem. Eng. J.* 2011, **170**, 82–89.

[12] G.X. Li, Y.M. Du, Y.Z. Tao, H.B. Deng, X.G. Luo, J.H. Yang, *Carbohyd. Polym*. 2010 **82**, 706.

[13] Y. Wang , X. Liu , H. Wang, G. Xi, W. Huang, R. Song. *J. Colloid Interface Sci*. 2014, **416**, 243.

[14] Y. Haldorai, J.-J. Shim. *Applied Surface Science* 2014, **292** 447.

[15] T. Kou, Y. Wang, C. Zhang, J. Sun, Z. Zhang. *Chemical Engineering Journal* 2013, **223**, 76.

[16] LIU Zhuannian, ZHOU Anning, WANG Guirong, ZHAO Xiaoguang. *Chinese Journal of Chemical Engineering*, 2009, **17(6),** 942.

[17] T.K. Saha, N.C. Bhoumik, S. Karmaker, M.G. Ahmed, H. Ichikawa, Y. Fukumori,. *J. Water Resour. Prot.* 2010, **2**, 898.

[18] A.J. Aishah, T.S. Sugeng, A. Hazirah, N.D. Rahim, M. Arif, A. Aziz,. *J. Hazard. Mater*. 2010, **181**, 755.

[19] W. Deligeer, Y.W. Gao, S. Asuha,. *Appl. Surf. Sci*. 2011, **257**, 3524.

[20] H.Y. Zhu, R. Jiang, Y.Q. Fu, J.H. Jiang, L. Xiao,. *Appl. Surf. Sci.*, 2011, **258**, 1337.

[21] Z.B. Hassina, B. Mokhtar, A. Loubna, *Chem. Eng. J*. 2012, **187**, 142.

[22] R. Huang, Q. Liu, J. Huo, B. Yang. *Arabian Journal of Chemistry*. 2013, IN PRESS.

[23] N. Mohammadi, H. Khani, V. Kumar Gupta, E. Amereh, S. Agarwal. *J. Colloid Interface Sci*. 2011, **362**, 457.

[24] A. Mittal, A. Malviya, D. Kaur, J. Mittal, L. Kurup. *J. Hazard. Mater.* 2007, **148**, 229.

[25] E. Haque, J. Eun Lee, I. Tae Jang, Y. Kyu Hwang, J.-S. Chang, J. Jegal, S. Hwa Jhung. *J. Hazard. Mater.* 2010, **181,** 535.

[26] Y. Tian, X. Wang, Y. Pan. *J. Hazard. Mater.* 2012, **213– 214**, 361.

[27] J.-H. Huang, K.-L. Huang, S.-Q. Liu, A-T.Wang, C. Yan. *Colloids and Surfaces A: Physicochem. Eng. Aspects* 2008, **330**, 55.

[28] G. Annadurai, R.S. Juang, D.J. Lee. *J. Hazard. Mater*. 2002, **B92**, 263.

[29] J. Liu, S. Ma, L. Zang. *Applied Surface Science.* 2013, **265,** 393.

[30] H. Chen, Ai. Zhong, J. Wu, J. Zhao, H. Yan. *Ind. Eng. Chem. Res*. 2012, **51**, 14026.

[31] X.S. Zhao, G.Q. Lu, X. Hu, *Microporous Mesoporous Mater*. 2000, **41**, 37.

[32] Y. Luo, J. Lin, *Microporous Mesoporous Mater*. 2005, **86**, 23.

[33] R. Wang, B. Gao, W. Jiao, *Appl. Surf. Sci*. 2009, **255**, 4109.

[34] R. Mukhopadhyay, S. Bhattacharjee, R. Bhattacharyya, *J. Chem. Soc., Dalton Trans.*, 1994, 2799.

[35] J. A. Cubillos, W. F. Hölderich. *Rev. Fac.Ing. Univ. Antioquia*. 2007, **41**, 31.

[36] J. Tedim, S. Patrício, R. Bessada, R. Morais, C. Sousa, M. B. Marques and C. Freire, *Eur. J. Inorg. Chem.*,2006, 3425.

[37] D.L. Griscom, R.E. Griscom. *J. Chem. Phys.* 1967, **47**, 2711.

[38] D.Y. Zhao, D. Goldfarb, in: L. Bonneviot, S. Kaliaguine (Eds.), Zeolites: A Refined Tool for Designing Catalytic Sites, Elsevier, Amsterdam, (1995) p. 181.

[39] G. Brouet, X. Chen, C.W. Lee, L. Kevan, *J. Am. Chem. Soc*. 1992, **114**, 3720.

[40] W.S. Kijlstra, E.K. Poels, A. Bliek, B. Weckhuysen, R.A. Schoonheydt, *J. Phys. Chem.* B 1997, **101**, 309.

[41] B. J. Aronson, Christopher F. Blanford, A. Stein, *J. Phys. Chem. B.* 2000, **104**, 449.

[42] V. Di Castro, G. Polzonetti, J*ournal of Electron Spectroscopy and Related Phenomena*, 1989, **48**, 117.

[43] C. Bauer, P. Jacques, A. Kalt. *Chem. Phys. Lett*. 1999, **307**, 397.

[44] H. Tamai, T. Yoshida, M. Sasaki, H. Yasuda. *Carbon* 1999, **37**, 983.

[45] R. Cheng, S. Ou, B. Xiang, Y. Li, Q. Liao *Langmuir* 2010, **26(2),** 752.

[46] Q. Zhang, Y. Wang, S. Itsuki, T. Shishido, K. Takehira, *J. Mol. Catal. A: Chem.* 2002, **188**, 189.

[47] R. S. Juang, J.Y. Chung, *J. Colloid Interface Sci*. 2004, **275** ,53.

[48] C.N.R. Rae. Chemical Applications of Infrared Spcctroscopy, Academic Press. New York. 1963, p. 337. 364.

[49] W. Ma, F. Q. Ya, M. Han, R. Wang. *J. Hazard. Mater.,* 2007, **143**, 296.